Structural phase transitions of cubic Gd_2O_3 at high pressures

F. X. Zhang, M. Lang, J. W. Wang, U. Becker, and R. C. Ewing*
Department of Geological Sciences, University of Michigan, Ann Arbor, Michigan 48109-1005, USA
(Received 19 February 2008; revised manuscript received 25 July 2008; published 22 August 2008)

An irreversible structural transformation from the cubic phase to a hexagonal high-pressure phase was verified in Gd_2O_3 between 7.0 and 15 GPa. The compressibility and bond distances of both phases were determined by the refinement of the x-ray diffraction data. The high-pressure phase of Gd_2O_3 is 9.2% denser than the cubic phase at 7 GPa. After release of pressure, the high-pressure phase transformed to a monoclinic structure. The pressure-induced phase transition from the monoclinic to the hexagonal phase is reversible. Unlike the case at atmospheric pressure, the hexagonal phase was found to transform to the monoclinic phase by increase of temperature at high pressures. The lattice potential energies and electronic density of states of the cubic, monoclinic, and hexagonal high-pressure phases of Gd_2O_3 were calculated from the known structural models with density-functional method. The observed phase stability, transition pressure, and volume change are well explained by theoretical calculations.

DOI: 10.1103/PhysRevB.78.064114 PACS number(s): 61.50.Ks, 72.80.Ga

I. INTRODUCTION

Sesquioxides play a vital role in the processing of ceramics as additives for low-temperature sintering, as grain growth inhibitors, and as phase stabilizers,[1] as well as potential applications in nuclear engineering.[2] Due to the photoluminescence properties of rare-earth elements, they are also important optical materials.[3,4] Depending on the radius of cation, there are three polymorphs for rare-earth sesquioxides at low temperatures: hexagonal phase (*A* type, space group: $P\text{-}3m1$) (rare-earth cations: La to Nd), monoclinic phase (*B* type, $C/2m$) (rare-earth cations: Sm to Gd), and cubic phase (*C* type, $Ia\text{-}3$) (other rare-earth cations). At very high temperature, there are additional two polymorphs in most rare-earth sesquioxides. One is hexagonal (*H* type) with lattice parameters close to those of the normal hexagonal phase, but in a different space group ($P6_3/mmc$), and another one is cubic (*X* type, $Im\text{-}3m$). The phase stability and phase transitions with temperature or pressure for all the rare-earth sesquioxides were summarized recently in Ref. 5. At ambient conditions, the crystal structure of most sesquioxides with cations of medium size depends on the thermal history; as an example, Gd_2O_3 can be either cubic or monoclinic at room conditions. With increase of temperature, phase transitions usually follow the sequence of $C \rightarrow B \rightarrow A$ for most Ln_2O_3 with medium size cations,[6–8] and the $C \rightarrow B$ and $B \rightarrow A$ phase transitions in Gd_2O_3 were reported at temperatures of ~1500 and 2443 K,[5] respectively. Hydrostatic pressure and shock-wave experiments have been performed on rare-earth sesquioxides using Raman scattering and x-ray diffraction (XRD) techniques before.[9–12] Recently, photoluminescence in Eu-doped Gd_2O_3 was studied under compression at room temperature and pressure-induced structural transitions were observed by energy-dispersive x-ray diffraction measurements.[13] A hexagonal structure was identified as the high-pressure phase. However, until this study, there is no detailed structural description for the high-pressure phase of Gd_2O_3 due to the energy-dispersive patterns or the poor quality angle-dispersive XRD data. The hexagonal phase *A* is regarded as the high-pressure phase, but there are not enough experimental results to support it because the hexagonal phases *A* and *H* of rare-earth sesquioxides have very close lattice parameters and XRD techniques cannot distinguish them. There are several reports on the Raman-scattering measurements for some of the sesquioxides before,[9,14] but Raman scattering, in fact, cannot distinguish the two hexagonal phases either.

Here, we report the outcome of a high-pressure study on cubic *C* form of Gd_2O_3 up to 43 GPa using *in situ* angle-dispersive XRD and Raman-scattering measurements. There is a pressure-induced phase transition between 7 and 15 GPa, and we provide a detailed structural description of this high-pressure phase based on a structural refinement of XRD data. The structural transformation between phases *B* and *A* was also investigated by *in situ* high-pressure and high-temperature XRD measurements for the first time. The phase transition between *B* and *A* under pressure is completely different from the case at atmospheric pressure. The monoclinic phase *B* is the most stable phase at high pressure and high temperature. The phase stabilities and phase transitions between *C*, *B*, and *A* were discussed in the context of quantum-mechanical calculations of the lattice potential energies of these phases.

II. EXPERIMENTAL DETAILS

The starting material of the cubic Gd_2O_3 was a commercial product (Alfa Aesar) with 99.9% purity. High-pressure experiments were performed in a diamond-anvil cell (DAC) with a culet size of 350 μm for the diamond anvils. A hardened stainless-steel gasket was indented to a thickness of 40 μm, and a hole with diameter of 100 μm drilled in the center served as sample chamber. In order to achieve good hydrostatic pressure conditions, only a limited amount of sample powder was used together with a methanol/ethanol/water mixture (16:3:1) pressure medium. Several ruby chips distributed throughout the sample chamber were used for pressure calibration by applying the standard ruby fluorescence method.[15] The measured pressure difference of various

 ©2008 The American Physical Society

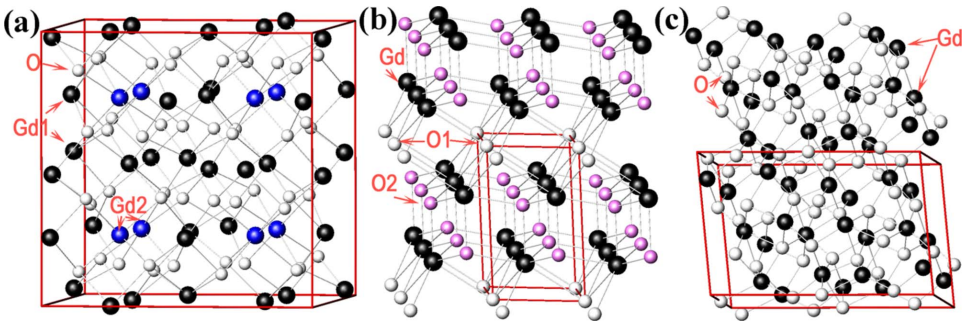

FIG. 1. (Color online) Crystal structures of Gd_2O_3 polymorphs (a) *C* cubic (*Ia*-3); (b) *A* hexagonal (*P*-3*m*1), and (c) *B* monoclinic (*C*2/*m*).

ruby chips was less than 2 GPa and the *R*1 and *R*2 peaks of the ruby fluorescence signal remained well separated up to a maximum pressure of 43 GPa, indicating that good quasihydrostatic pressure conditions were guaranteed even at high pressures when the pressure medium solidified. *In situ* XRD measurements were conducted at the X 17C station of the National Synchrotron Light Source, Brookhaven National Laboratory. A monochromatic beam with wavelength of 0.4066 Å was used, focused to a spot of about 25 μm in size.

The *in situ* pressure/temperature experiments were performed in a resistant heated DAC with Re gasket and without pressure transmitting medium. The temperature was monitored with a *K* type thermocouple and the temperature deviation is less than 10 K during measurement. The XRD patterns were recorded at B2 station of Cornell High Energy Synchrotron Source (CHESS) with x-ray wavelength of 0.496 Å. Debye rings were recorded with a Mar charge coupled device (CCD) detector and the integrated two-dimensional patterns were obtained from images by using the software FIT 2D.[16] XRD patterns of the various polymorphs of Gd_2O_3 were refined by the Rietveld method[17] based on the known structural models.[6] The Raman spectrum was recorded with a confocal micro-Raman instrument (Spex 270 M) attached with a liquid nitrogen cooled CCD detector. The activation light is from an Ar laser with wavelength of 514 nm. The quantum-mechanical calculations were performed within the density-functional theory (DFT) framework with

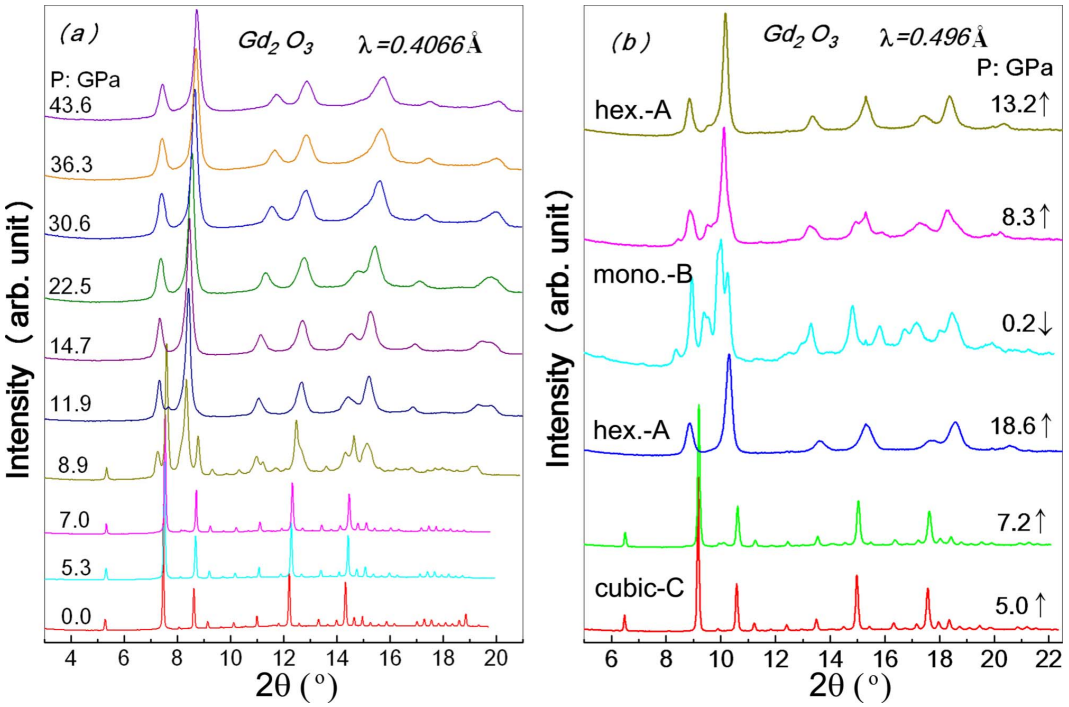

FIG. 2. (Color online) (a) XRD patterns of Gd_2O_3 with increasing pressure. A pressure-induced structural transition can be observed, which begins at ~7 GPa and is complete at ~15 GPa. (b) The high-pressure hexagonal phase transformed to monoclinic phase after release of pressure and the phase transition from the monoclinic to the hexagonal phase is reversible and has a little lower transition pressure (6.8 GPa) compared with that of the cubic to hexagonal phase transition. The diffraction patterns for the high-pressure phase show a broadening in peak width. The patterns marked with "cubic *C*," "mono. *B*" or "hex. *A*" are contributed by a single phase, and unmarked patterns are mixture of two phases. The up and down arrows represent the loading and unloading processes.

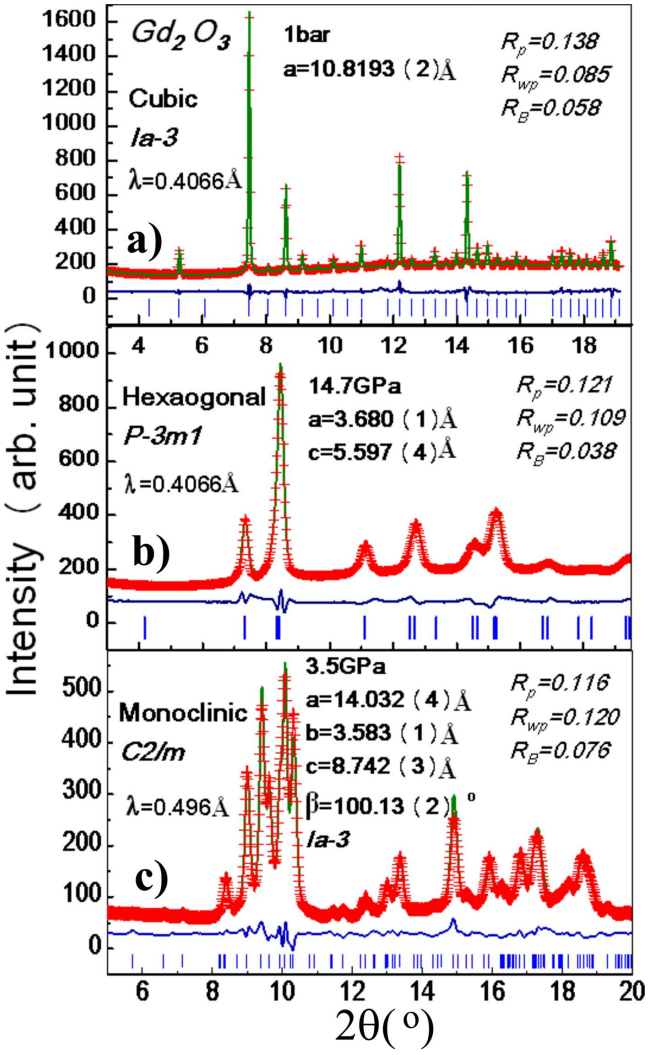

FIG. 3. (Color online) Rietveld refinement of the XRD pattern of Gd_2O_3 (a) at ambient conditions with space group of Ia-3; (b) the high-pressure phase at pressure of 14.7 GPa with space group of P-3m1; (c) the monoclinic phase at 3.5 GPa (after annealing at high pressure) with space group of $C2/m$.

plane-wave basis set implemented in the Vienna Ab-initio Simulation package.[18]

III. RESULTS AND DISCUSSION

The schematic crystal structure of cubic Gd_2O_3 is shown in Fig. 1(a). There are two Gd sites in the unit cell: the 8b site, which is octahedrally coordinated with six oxygen atoms, and another at the 24d site, which has four shorter and two longer bond distances with O. The refinement of the XRD pattern recorded at room conditions [Fig. 3(a)] gives a lattice constant of 10.8193(2) Å, which is in good agreement with the literature values.[10,19] The selected XRD patterns of Gd_2O_3 with increasing pressure are shown in Fig. 2, and the cubic structure is stable up to 7 GPa, which is a little lower than that measured with energy-dispersive XRD in nanosized material.[13] At higher pressures, the appearance of new diffraction peaks in the XRD patterns (Fig. 2) indicates a pressure-induced structural transformation. The phase transition is complete below 15.3 GPa, and the high-pressure phase can be indexed as hexagonal. The two hexagonal polymorphs (A and H) of rare-earth sesquioxides have similar lattice parameters, but different symmetries. The XRD cannot distinguish them at all, but they were identified by neutron diffraction before.[8] The H phase was proposed to describe the high-temperature phase (>2443 K), and all the atomic sites in the unit cell are half-occupied and the molar volume of the high-temperature phase is larger than that of the low-temperature phase due to lattice expansion. In contrast, high-pressure phase usually has a smaller molar volume, and partial occupancy of so many sites as H phase seems unlikely to appear in a high-pressure phase. Thus, the XRD patterns for the high-pressure phase were refined based on space group of P-3m1. Figure 1(b) shows the crystal structure of the hexagonal phase (P-3m1), and all three independent sites in the unit cell are fully occupied. The calculated XRD pattern fits the observed patterns very well. Figure 3(b) shows the observed and calculated XRD patterns at 14.7 GPa, and the refined lattice parameters are $a=b=3.680(1)$ Å and $c=5.597(4)$ Å. The details of the structural data of the high-pressure phase of Gd_2O_3 at 14.7 GPa are given in Table I.

The normalized lattice parameters of the cubic and hexagonal phases from the refinement are shown in Fig. 4. Note, the hexagonal unit cell has an extremely anisotropic compressibility. The relative change along the c axis is approximately 5.7 times larger than that along the a or b axis from 10 to 43 GPa. This anisotropic compressibility is often observed in compounds with layered structures,[20–22] which have weak van der Waals bonds between the atoms in adjacent layers. The anisotropic compressibility of the hexagonal Gd_2O_3 indicates that the high-pressure phase may have a layerlike structure, and the bonding between layers is weak as compared with the ⟨Gd-O⟩ bond within the same layer. The pressure dependence of the unit-cell volume for Gd_2O_3 is shown in Fig. 4(b). There is 9.2% volume shrinkage dur-

TABLE I. Atomic coordinates of the hexagonal Gd_2O_3 at 14.7 GPa. The refinement of the XRD pattern with $a=b=3.680(1)$ Å, $c=5.597(4)$ Å, and space group P-3m1 (164) results in fitting $R_p=12.1\%$, $R_{wp}=10.9\%$, $R_{\text{Bragg}}=3.75\%$, and $R_f=3.97\%$.

Atom	Position	x/a	y/b	z/c	Occupancy
Gd	2d	1/3	2/3	0.253(7)	1
O1	2d	1/3	2/3	0.653(9)	1
O2	1a	0	0	0	1

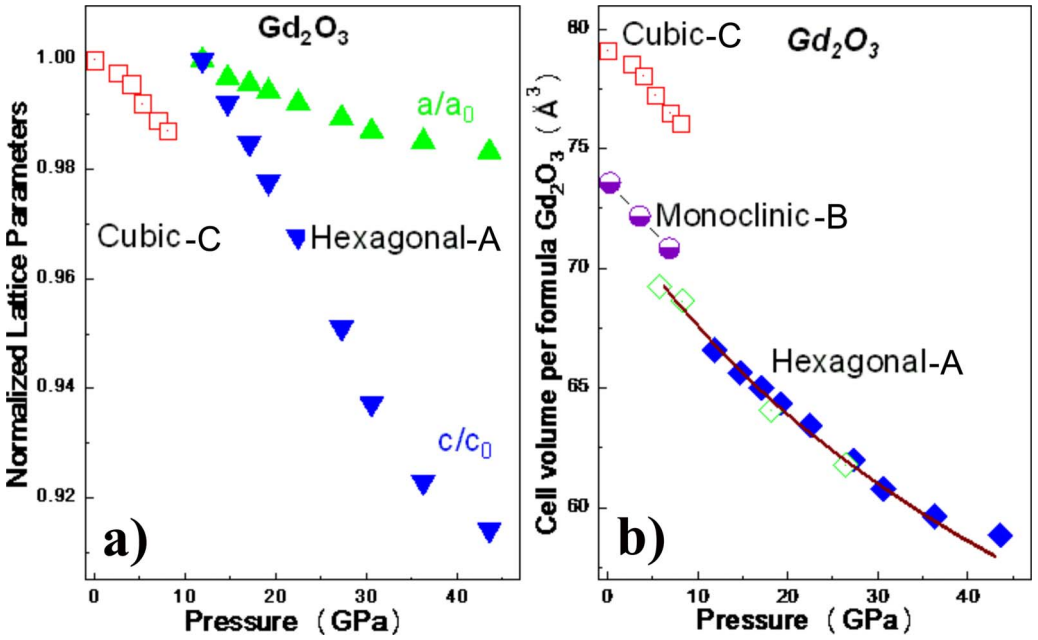

FIG. 4. (Color online) Pressure dependence of (a) normalized lattice parameters of Gd_2O_3; (b) unit-cell volume of every formula Gd_2O_3. A volume decrease of 9.2% can be observed during the transition from the cubic to the hexagonal structure at 7 GPa. The unit-cell volume of monoclinic *B* form is between that of cubic *C* form and hexagonal *A* form, but close to phase *A*. The open symbols in (b) were measured during pressure release. The solid line is the fitting with Birch-Murnaghan equation of state.

ing the phase transition at ~7 GPa. Fitting the *P-V* curve with a Birch-Murnaghan equation of state yielded a bulk modulus of 188(25) GPa and 160(21) GPa for the cubic and hexagonal phases, respectively, when the pressure derivative at zero pressure was fixed at $B_0'=4$. The similar values of bulk modulus for the cubic and hexagonal Gd_2O_3 reveal that the high-pressure phase of Gd_2O_3 has similar compressibility with that of the cubic phase. A similar behavior was also observed in Sm_2O_3 recently.[23] The diffraction peaks with two theta diffraction angle of 15°–16° at pressures above 30 GPa are completely overlap, which may suggest another phase transition. However, all the XRD patterns of the high-pressure phase up to 43.6 GPa can be refined with the same hexagonal structural model, even though there is a small discontinuity in the slope of the volume-pressure curve [Fig. 4(b)].

The bonding environment of the cubic and the hexagonal phases was analyzed using the refinement of the XRD patterns. The ⟨Gd-Gd⟩ and ⟨Gd-O⟩ bond distances in both phases and their pressure dependences are shown in Fig. 5. For the cubic phase, there are two Gd sites in the unit cell; the ⟨Gd-Gd⟩ bond distances change almost linearly with the decrease of lattice parameter from ~3.60 Å at ambient pressure to ~3.57 Å at 7 GPa. The bond distance of ⟨Gd-O⟩ in the cubic phase shows a more complicated behavior with increasing pressure, varying between 2.22 and 2.37 Å. For the hexagonal phase, there is only one Gd site, but two O sites in the unit cell. The bond distance between cations parallel to the *a-b* plane and along the *c* axis shows different behaviors with increasing pressure [Fig. 5(a)]. The former has no big change in the whole pressure range, while the latter decreases dramatically with the increase of pressure above 17 GPa. This is in agreement with the strong anisotropic compressibility of the hexagonal unit cell. The ⟨Gd-Gd⟩ bond distance along the *c* axis decreases from ~3.50 Å at ~15 GPa to 3.16 Å at 44 GPa. Each Gd atom in the hexagonal phase bonds with seven oxygen atoms, in which three oxygen atoms (O1) reside on the corner of the unit cell, three oxygen atoms (O2) are nearly in the same plane paralleling to the *a-b* plane, and the seventh oxygen (O2) is in the neighboring layer [Fig. 1(b)]. Both of the bond lengths between Gd and O, which reside on the corner of the unit cell, and O2 in the same layer slightly decrease with the increase of pressure. However, the bond length between Gd and the seventh oxygen (O2) in the neighboring layer increases with pressure from 2.15 Å at ~11 GPa to 2.45 Å at ~30 GPa. This indicates that hexagonal Gd_2O_3 becomes more layerlike with the increase of pressure. XRD results reveal that all the cation-anion bond distances have no apparent change above 30 GPa except the slight decrease of the bond length between Gd and the seventh oxygen (O2).

The structural phase transition of Gd_2O_3 was also studied using *in situ* Raman scattering at high pressures. Based on group theory analysis,[14,23] the cubic Gd_2O_3 has totally 26 Raman-active modes at the Brillouin center $\Gamma=4A_g+4E_{1g}+4E_{2g}+14T_g$, and there are only four Raman-active modes for the high-pressure phase $\Gamma=2A_{1g}+2E_g$. The strongest mode for the cubic Gd_2O_3 is centered at 362 cm^{-1}, and most of the Raman modes in the cubic phase can be observed at atmospheric pressure (Fig. 6). With increasing pressure, however, only the strongest Raman mode remained clearly observable. At a pressure of 11.2 GPa, this strong mode nearly disappeared, indicating a pressure-induced phase transition, which is in good agreement with the XRD data. The Raman signal of the high-pressure phase was very weak and only two peaks were observed at frequency around

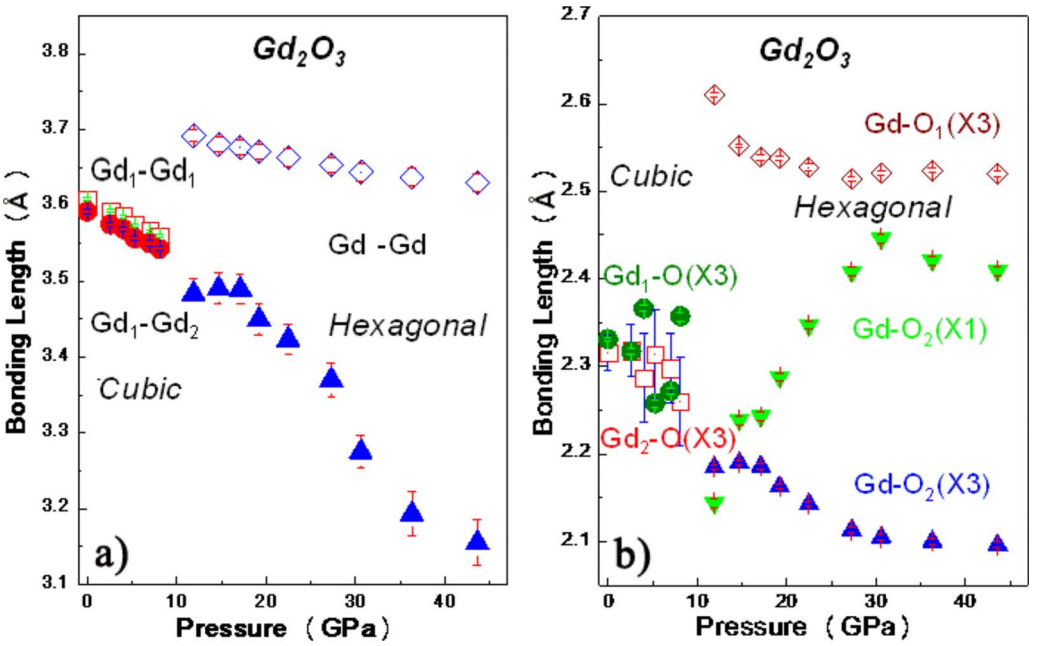

FIG. 5. (Color online) Pressure dependence of bond-distances in the cubic and the hexagonal high-pressure phases of Gd_2O_3 (a) ⟨Gd-Gd⟩ and (b) ⟨Gd-O⟩. Numbers in the brackets represent numbers of bonds in the unit cell.

500 cm^{-1}. These two modes are similar with the stretching modes observed in the high-pressure phase of Sm_2O_3.[14] The Raman-active modes for the high-pressure phase of Gd_2O_3 were too weak to be detected at pressures higher than 14 GPa with our facility. The sample quenched from 30 GPa showed a completely different Raman spectrum from the starting material. As compared with the reported Raman spectrum of other rare-earth sesquioxides,[8] the quenched sample has a monoclinic structure. Thus, the hexagonal high-pressure phase of Gd_2O_3 is not stable and underwent a phase transformation during decompression. The XRD measurements of the quenched sample also confirmed its monoclinic structure. These results give a clear explanation for why only the cubic-to-monoclinic ($C \rightarrow B$) phase transition has been observed by shock wave or other *ex situ* high-pressure measurements on some rare-earth sesquioxides before.[9] The high-pressure phase of Gd_2O_3 is not quenchable, and *ex situ* measurements cannot reveal the details of pressure-induced phase transitions.

Recently, Guo *et al.*[24] has studied a similar oxide Sm_2O_3 with mixture phases of *C* and *B* as the starting material at high pressure with energy-dispersive XRD measurements and theoretical calculations. Phase transitions from both *C* and *B* to *A* were identified. In order to detect the phase stability and phase transitions between *C*, *B*, and *A*, we performed several cycles of loading and unloading pressure experiments at room temperature. In a separate experiment in CHESS, a similar pressure-induced *C* to *A* phase transition was confirmed at 7.2 GPa [Fig. 2(b)]. The sample of Gd_2O_3 at 18.6 GPa was the pure high-pressure phase and a monoclinic phase (*B*) was detected when the pressure was released down to 0.2 GPa. The refinement of the XRD pattern yields lattice parameters of $a=14.14(2)$ Å, $b=3.618(3)$ Å, $c=8.76(1)$ Å, and $\beta=99.91(9)°$ for the monoclinic phase, which are very close to the values in the literature.[25] The phase transition from *B* to *A* was found starting at 6.8 GPa and the transformation was nearly completed at 13.2 GPa.

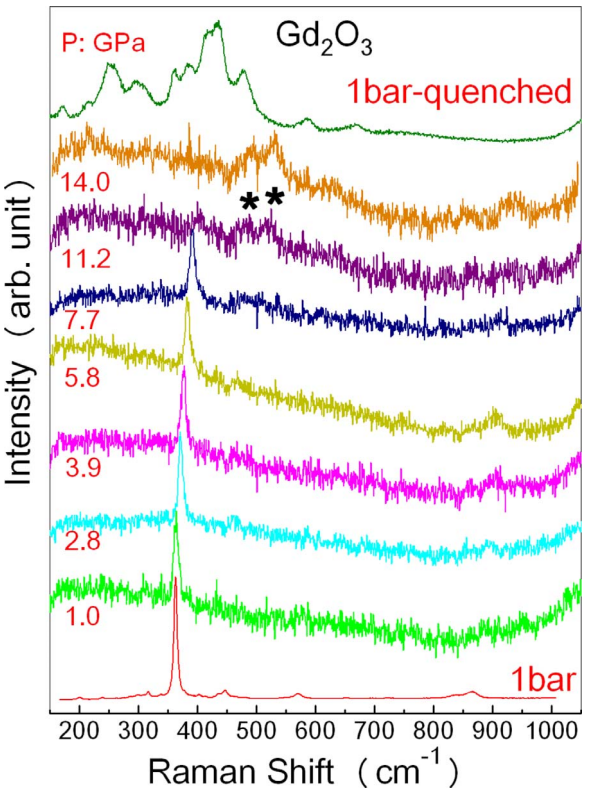

FIG. 6. (Color online) Raman spectra of Gd_2O_3 with increasing pressure up to 14.0 GPa together with a spectrum of the recovered sample. The phase transition is indicated by the absence of the strong Raman mode of the cubic phase and the observation of the weak peaks of the high-pressure phase marked with asterisks. The recovered sample is monoclinic.

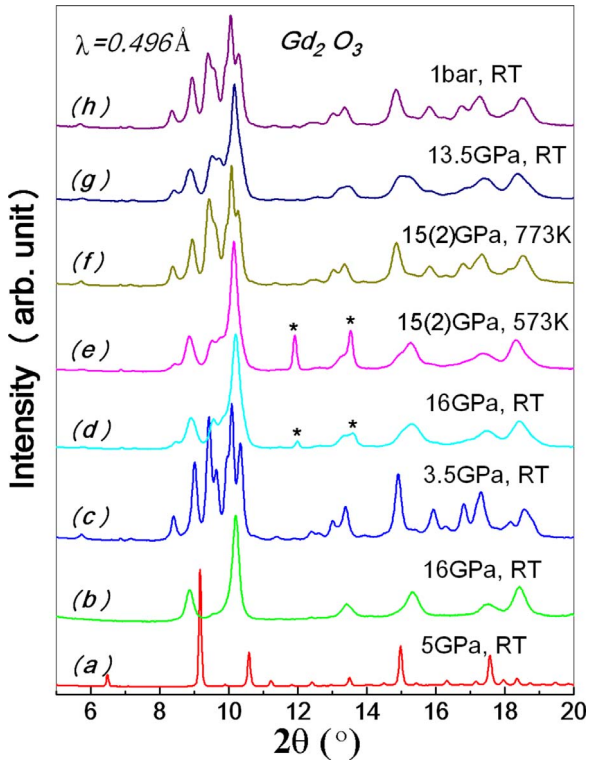

FIG. 7. (Color online) Selected XRD patterns of Gd_2O_3 at different pressure and temperatures. (a) and (b) are the patterns at room temperature and at 5.0 and 16.0 GPa, respectively. (c) is the pattern measured at room temperature after the sample was heated at 773 K for 1 h at 8.5 GPa. The pressure fell down to 3.5 GPa during heating. (d)–(g) represent the patterns for the above sample compressed to 16.0 GPa and measured at RT, 573 K, 773 K, and RT (after cooling down and pressure fell down to 13.5 GPa), respectively. (h) is the pattern of the quenched sample.

Our XRD measurements during several cycles of loading and unloading pressure processes verified the pressure-induced phase transition between *B* and *A* phase is reversible.

At normal pressure, phase *A* is only stable at high temperature (>2443 K to Gd_2O_3, see Ref. 5 and references therein) and it is expected that temperature should enhance the phase transitions of C→A or B→A. However, we observed a different phase-transition behavior for Gd_2O_3 at high pressure and high temperature. High-pressure/high-temperature experiments were applied in a heatable DAC with resistance heating. Figure 7 shows the XRD patterns of Gd_2O_3 measured at different pressures and temperatures. At room temperature [Figs. 7(a) and 7(b)], a similar *C* to *A* phase transition was observed without pressure medium. The sample was compressed to 25 GPa in order to make sure the formation of the pure hexagonal phase. Then the pressure was released to about 8.5 GPa, which is still above the critical pressure of phase transition from *C* to *A*, and heated the sample at 773 K for 1 h. After heating, the pressure fell down to 3.5 GPa due to the thermal relaxation and the XRD pattern indicated a well-crystallized monoclinic structure [Fig. 7(c)]. We refined the structure with the monoclinic Sm_2O_3 structural model and the fitting results, and structural parameters are shown in Fig. 3(c) and listed in Table II, respectively. The monoclinic phase was then compressed to 16 GPa again at room temperature and the structure is mainly the hexagonal phase with minor *B* phase [Fig. 7(d)]. The sample was then heated at this pressure and the XRD patterns were taken at 423, 573, and 773 K, respectively. We found that the high-pressure phase was not grown with increase of temperature. On the contrary, more monoclinic phase was observed at temperature higher than 573 K from the XRD pattern and a pure *B* phase was observed at 773 K [Fig. 7(f)]. The temperature-induced phase transition between *A* and *B* is also reversible at high pressures. The XRD pattern for the sample cooled down to room temperature at this pressure (the pressure fell down to 13.5 GPa during heating) mainly contained the hexagonal phase [Fig. 7(g)]. The quenched sample was completely the monoclinic phase *B*. The observed temperature-induced *A* to *B* phase transition at high pressure is difficult to be understood. As the phase *A* is a high-temperature phase and phase transition from *B* to *A* was reported in Gd_2O_3 at temperature higher than 2443 K at atmospheric pressure.[5] At high pressures, the process is reverted and not very high temperature (e.g., <773 K) can induce the *A* to *B* phase transition.

The electron density of state of Gd_2O_3 at atmospheric pressure was calculated with quantum-mechanical theory

TABLE II. Atomic coordinates (the atomic coordinates of O are not refined) of the monoclinic Gd_2O_3 at 3.5 GPa. The sample is first compressed to 25 GPa, then release pressure to 8 GPa and followed by *in situ* heating at 873 K for one hour. The refinement of the XRD pattern yields lattice parameters of a =14.032(4) Å, b=3.583(1) Å, c=8.742(3) Å, and β=100.13°. The residual parameters are R_p=11.6%, R_{wp}=12%, and R_B=7.65%.

Atom	Position	x/a	y/b	z/c	Occupancy
Gd1	4*i*	0.1406(19)	1/2	0.5117(21)	1
Gd2	4*i*	0.1934(14)	1/2	0.1653(19)	1
Gd3	4*i*	0.4655(11)	1/2	0.2059(16)	1
O1	4*i*	0.1289	0	0.2864	1
O2	4*i*	0.3250	1/2	0.0265	1
O3	4*i*	0.2984	1/2	0.3738	1
O4	4*i*	0.4741	0	0.3438	1
O5	2*b*	0	1/2	0	1

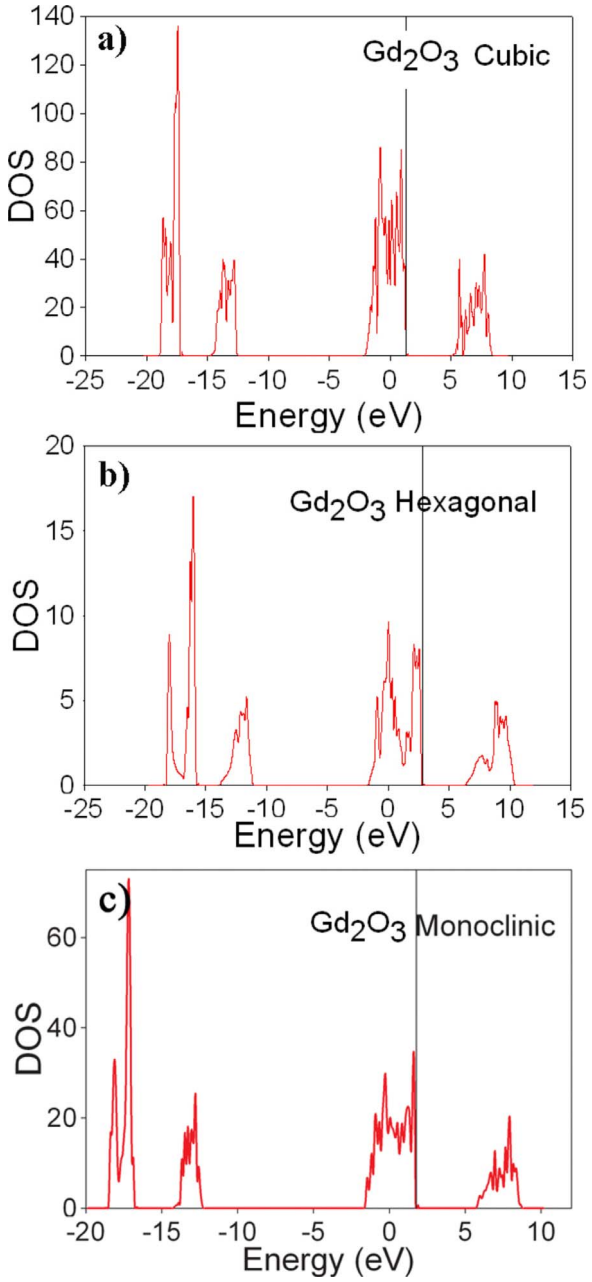

FIG. 8. (Color online) Calculated dispersive curve in the Brillouin zone, and the electron density of states (DOS) for the cubic, hexagonal, and monoclinic phases of Gd_2O_3.

and the results are shown in Fig. 8. At ambient pressure, all the three phases (A, B, and C) of Gd_2O_3 are nonconductive. The polymorphs have similar density of states and the band gaps are 3.60, 3.70, and 3.56 eV for the cubic C, monoclinic B, and hexagonal A phases, respectively. The dependence of lattice potential energy on the molar volume for the cubic, monoclinic, and hexagonal Gd_2O_3 was calculated and is shown in Fig. 9. The unit-cell volume at the lowest energy for the three phases fits the measured volumes at room conditions quite well. The hexagonal and monoclinic phases have smaller molar volumes as compared with the cubic phase. The monoclinic Gd_2O_3 has the highest lattice energy and it should be a high-temperature phase and the reported

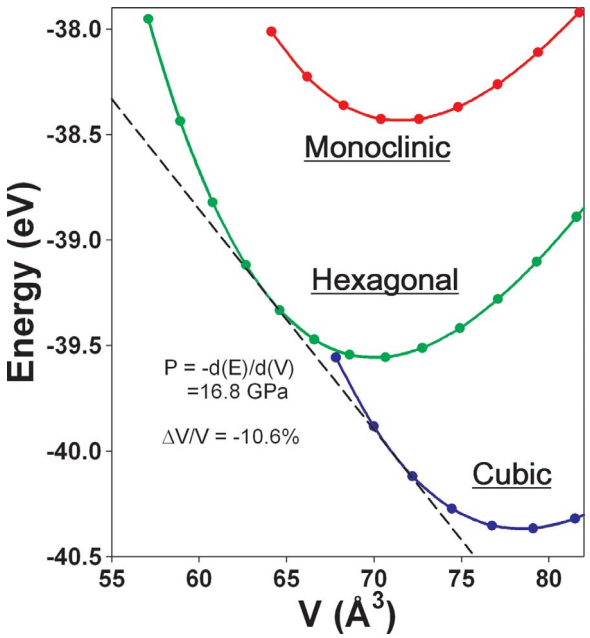

FIG. 9. (Color online) The calculated lattice energies of Gd_2O_3 in the cubic, hexagonal, and monoclinic structures. The transition pressure of $C \rightarrow A$ is 16.8 GPa. The monoclinic phase B is a high-temperature phase and phase transition of $C \rightarrow B$ should never happen for Gd_2O_3 because the formation of A phase at high pressure.

$C \rightarrow B$ phase transition for Gd_2O_3 at atmospheric pressure is around 1500 K.[5,6] The calculated transition pressure for $C \rightarrow A$ is ~16.8 GPa, which is a little larger than the observed value, and there is a decrease in volume of 10.6% from the cubic to the hexagonal structure. The calculated phase stabilities of the two polymorphs are in good agreement with experimental observations. The calculated lattice energy of the monoclinic phase of Gd_2O_3 is much higher than that of the C phase. From the calculated lattice energy curve in Fig. 9, B is a high-temperature phase and phase transition of $C \rightarrow B$ cannot be realized by pressure at low temperature. However, the $C \rightarrow B$ phase transition may become possible at high temperature and high pressure.

The phase stability and thermodynamic properties of rare-earth sesquioxides at high temperature were widely investigated and temperature-induced phase transitions of $C \rightarrow B$ or $B \rightarrow A$ (or H) were identified many years ago.[5,26–28] Similarly, pressure-induced phase transitions from C to B or A were also reported before by Raman or XRD experiments and the transition pressure ranged from several gigapascal to more than 10 GPa in many rare-earth sesquioxides.[1,9,29–31] From understanding in atomic scale, the temperature-induced phase transition between C and B is reconstructive and B to A is displacive. Though the $C \rightarrow B$ phase transition at high temperature is reversible, the revised phase transition usually needs a long-time heat treatment because the reconstruction of lattice has a large energy barrier. At normal pressure, no $C \rightarrow A$ phase transition was observed by temperature. At high pressure, only $C \rightarrow A$ transition and no $C \rightarrow B$ transition was observed in Gd_2O_3. This can be easily understood from the energy curves in Fig. 9 because of the large energy difference between phases C and B The monoclinic Gd_2O_3 is a

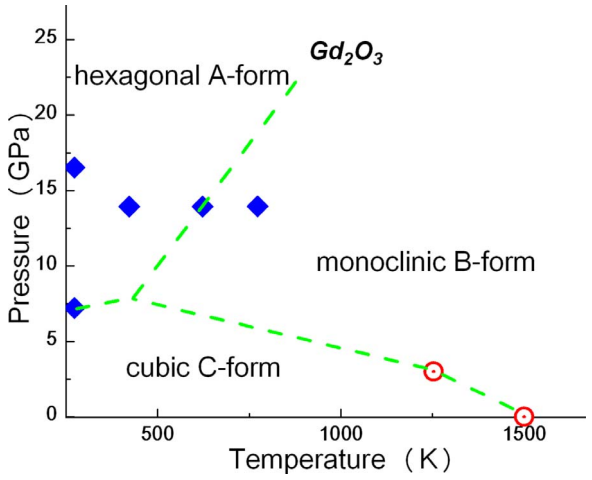

FIG. 10. (Color online) Schematic phase diagram of Gd_2O_3 at high pressure and high temperature. Open symbols resent the data taken from Refs. 6 and 31.

high-temperature phase and there may be a cotangent line between the energy curves of C and B, but it occurs at very high pressure, which is much larger than the formation pressure of the hexagonal phase. In addition, phase A usually has a smaller molar volume than phase B and pressure is thus favorable for the formation of phase A. However, pressure-induced $C \rightarrow B$ phase transition was reported before in some sesquioxides with small size cations such as Sc_2O_3, Y_2O_3, and Sm_2O_3.[9,10] The observed phase transition of $C \rightarrow B$ in Sm_2O_3 with shock wave[10] may not take place during pressuring process because recent *in situ* XRD measurements[24] did not found the $C \rightarrow B$ phase transition in the system. The lattice energy curve and phase stability of sesquioxides with small size cations may be different from the case of Gd_2O_3. From the results of our experiments and literatures, a possible P-T phase diagram for Gd_2O_3 is illustrated in Fig. 10. The monoclinic phase B is a high-temperature phase. At atmospheric pressure, the temperature for $C \rightarrow B$ phase transition is around 1500 K. At high pressures (<7 GPa), the transition temperature is much lower. To Sc_2O_3, Y_2O_3, or other sesquioxides with small size cations, the C phase is stable till to its melting point. The $C \rightarrow B$ boundary will parallel the x axis in Fig. 10, and the three phase point Γ will move toward the y axis. Once Γ moves below room temperature, the pressure-induced phase transitions $C \rightarrow B \rightarrow A$ become possible to these systems at room temperature. The phase transition of $C \rightarrow A$ is reconstructive, and the broad width of the diffraction peaks of phase A in Fig. 2 is not due to the nonhydrostatic conditions, but due to the very small grain size. It is not expected the grain growth of the high-pressure phase at room temperature. After phase transition occurred, the cubic phase cannot be recovered because of the large energy barrier. The monoclinic phase B is a metastable phase to Gd_2O_3 and the $B \rightarrow A$ phase transition at room temperature cannot be explained directly from the energy curves in Fig. 9. The phase transition between B and A only needs "displacement" of atoms (smaller energy barrier), but the phase transition between them is not so quick in Gd_2O_3 and the two phases coexisted over a pressure range of more than 5 GPa. In general, phase transition is controlled by both energy barrier of phase transition and difference of lattice energies. When the temperature is more than 773 K, the energy barrier between phases B and A is not important to Gd_2O_3, and phase B may have a lower energy and become the most stable phase at high pressure and high temperature.

IV. SUMMARY

The structure of Gd_2O_3 was studied at high pressure up to 43 GPa by *in situ* XRD and Raman measurements. The pressure-induced phase transition from the cubic phase to a high-pressure polymorph occurred at ~ 7 GPa and was complete at pressure below 15 GPa. The refinement results suggest that the structure became more layerlike with the increase of pressure. There is a volume decrease of about 9.2% during the phase transition at 7 GPa, and the high-pressure phase cannot be quenched to ambient conditions. During the process of decompression, the hexagonal high-pressure phase transformed to a monoclinic structure. The monoclinic phase B of Gd_2O_3 is a high-temperature phase and the phase transition between B and A is reversible by pressure and/or temperature. The observed pressure-induced phase transitions in Gd_2O_3 are in good agreement with quantum-mechanical calculations of the lattice energies of the hexagonal (A), monoclinic (B), and cubic (C) structures.

ACKNOWLEDGMENTS

This work was supported by the Office of Basic Energy Sciences of the U.S. Department of Energy, through Grant No. DE-FG02-97ER45656 and the NSF NIRT program (EAR-0403732). The use of the National Synchrotron Light Source at X 17C station is supported by NSF COMPRES Contract No. EAR01-35554 and by U.S. DOE Contract No. DE-AC02-10886. The use of CHESS beam is supported by the NSF and NIH/NIGMS via NSF Grant No. DMR-0225180.

*rodewing@umich.edu

[1] V. Srikanth, A. Sato, J. Yoshimoto, J. H. Kim, and T. Ikegami, Cryst. Res. Technol. **29**, 981 (1994).
[2] M. Tang, P. Lu, J. A. Valdez, and K. E. Sickafus, J. Appl. Phys. **99**, 063514 (2006).
[3] L. Laversenne, Y. Guyot, C. Goutaudier, M. Th. Cohen-Adad, and G. Boulon, Opt. Mater. **16**, 475 (2001).
[4] J. Zarembowitch, J. Gouteron, and M. Lejus, J. Raman Spectrosc. **9**, 263 (1980).
[5] M. Zinkevich, Prog. Mater. Sci. **52**, 597 (2007).
[6] H. R. Hoekstra and K. A. Gingerich, Science **146**, 1163 (1964).
[7] A. Bartos, K. P. Lieb, M. Uhrmacher, and D. Wiarda, Acta Crys-

tallogr., Sect. B: Struct. Sci. **49**, 165 (1993).
[8] P. Aldebert and J. P. Traverse, Mater. Res. Bull. **14**, 303 (1979).
[9] E. Husson, C. Proust, P. Gillet, and J. P. Itie, Mater. Res. Bull. **34**, 2085 (1999).
[10] T. Atou, K. Kusaba, K. Fukuoka, M. Kikuchi, and Y. Syono, J. Solid State Chem. **89**, 378 (1990).
[11] A. Atou, K. Kusaba, Y. Tsuchida, W. Utsumi, T. Yagi, and Y. Syono, Mater. Res. Bull. **24**, 1171 (1989).
[12] H. R. Hoekstra and K. A. Gingerich, Science **146**, 1163 (1964).
[13] H. Chen, C. He, C. Gao, J. Zhang, S. Gao, H. Lu, Y. Nie, D. Li, S. Kan, and G. Zou, Chin. Phys. Lett. **24**, 158 (2007).
[14] T. Hongo, K. I. Kondo, K. G. Nakamura, and T. Atou, J. Mater. Sci. **42**, 2582 (2007).
[15] H. K. Mao, J. Xu, and P. M. Bell, J. Geophys. Res. **91**, 4673 (1986).
[16] A. P. Hammersley, *Fit 2d* (ESRF, Grenoble, France, 1998).
[17] J. Rodriguez-Carvajal, FULLPROF 2K, France, 2001.
[18] G. Kresse and J. Furthmuller, Phys. Rev. B **54**, 11169 (1996).
[19] A. Saiki, N. Ishizawa, N. Mizutani, and M. Kato, J. Ceram. Soc. Jpn. **93**, 649 (1985).
[20] F. X. Zhang, S. K. Saxena, and C. S. Zha, J. Solid State Chem. **180**, 1759 (2007).
[21] F. X. Zhang, J. W. Wang, U. Becker, J. Lian, J. Hu, S. Saxena, and R. C. Ewing, J. Am. Chem. Soc. **129**, 13923 (2007).
[22] F. X. Zhang, J. Lian, U. Becker, R. C. Ewing, L. M. Wang, J. Hu, and S. K. Saxena, J. Solid State Chem. **180**, 571 (2007).
[23] J. Zarembowitch, J. Gouteron, and A. M. Lejus, Phys. Status Solidi B **94**, 249 (1979).
[24] Q. X. Guo, Y. Zhao, C. Jiang, W. L. Mao, and Z. W. Wang, Solid State Commun. **145**, 250 (2008).
[25] JCPDF Card Nos. 42-1465 and 43-1015.
[26] J. Coutures and M. Foex, J. Solid State Chem. **11**, 294 (1974).
[27] J. Coutures, F. Sibieude, and M. Foex, J. Solid State Chem. **17**, 377 (1976).
[28] J. Coutures, A. Rouanet, R. Verges, and M. Foex, J. Solid State Chem. **17**, 171 (1976).
[29] H. R. Hoekstra, Inorg. Chem. **5**, 754 (1966).
[30] H. A. Seck, F. Dachille, and R. Roy, Inorg. Chem. **8**, 165 (1969).
[31] R. J. M. Konings, J. C. van Miltenburg, and A. C. G. Van Genderen, J. Chem. Thermodyn. **37**, 1219 (2005).